Electron-localization mechanisms in $GaAs/Ga_{0.7}Al_{0.3}As$ superlattices

Mark Lee, S. A. Solin, and D. R. Hines
NEC Research Institute, Princeton, New Jersey 08807
(Received 25 November 1992; revised manuscript received 29 April 1993)

The effects of miniband width (Δ), applied electric field, and atomic layering thickness disorder present in real semiconductor superlattices (SL's) have been studied experimentally via transverse magnetotransport experiments on a set of n-type modulation-doped $GaAs/Ga_{0.7}Al_{0.3}As$ SL's. X-ray diffraction and transmission-electron microscopy studies show that the thickness of any given layer may vary randomly by ± 1 atomic monolayer from the well-defined average layer thickness. Current-voltage traces show a large drop in the high-field differential conductivity with a characteristic voltage that is proportional to Δ in the range $10 < \Delta < 30$ meV, but which is nearly independent of Δ for $\Delta \gtrsim 30$ meV. This behavior is consistent with a crossover from a Wannier-Stark to a negative effective-mass field-induced localization mechanism. Furthermore, magnetotransport data at low temperatures clearly show small disorder-induced localization corrections to the conductivity in the smaller bandwidth SL's. Scattering length scales derived from the data indicate that the dominant source of disorder is the layer thickness variations. This disorder introduces a mobility edge which is smaller than Δ in the samples studied, but which is comparable to the Fermi energy so that the smallest bandwidth SL is very near a metal-insulator transition.

I. INTRODUCTION

Since the advent of atomically controlled thin-film growth techniques, artificially structured superlattice (SL) systems have had broad appeal both for their possible electronic device applications and for their potential to open previously inaccessible regimes in solid-state physics. The paradigm SL is the $GaAs/Ga_{1-x}Al_xAs$ system grown by molecular-beam epitaxy (MBE), where essentially perfect lattice-matched interfaces and nearly defect-free crystalline quality over macroscopic length scales are now routinely achieved. Beginning with the pioneering work of Esaki and Chang,[1] studies of electron transport through these types of SL's have yielded a great deal of new physical insight, primarily because factors such as the periodicity, carrier concentration and polarity, and band properties can be designed and controlled in a manner not possible with more conventional crystalline or amorphous materials. Furthermore, parameters such as the size of the SL Brillouin zone and miniband width (Δ) can take on values considerably smaller than with bulk lattices, which has allowed several old and fundamental questions[2] regarding high-field electron transport in a periodic system to be experimentally addressed in a direct manner. Also, as the nature of electron transport through SL's is important to the operation of devices such as band-gap-engineered transistors[3] and surface-emitting lasers,[4] it is important to understand how imperfections that still appear in MBE growth might affect the physics of conduction in real SL's.

We report the results of experiments aimed at understanding what intrinsic and extrinsic conditions might limit the simple semiclassical picture of ohmic electron transport through $GaAs/Ga_{0.7}Al_{0.3}As$ SL's, as a function of electric field, magnetic field, and temperature. Recent work by Sibille *et al.*,[5] Beltram *et al.*,[6] and Tsu and Esaki[7] on the competition between scattering and bandwidth in high-electric-field-induced localization in SL's has suggested a more unified concept of this phenomenon. The data presented here support at least the general picture constructed by these authors. Furthermore, inhibition of exciton propagation through SL's was observed in the photoluminesence experiments of Capasso *et al.*,[8] and Chomette *et al.*,[9] who attributed it to disorder-induced localization of the holes resulting from layer thickness variations. Here we show that such disorder can serve to localize electrons when the SL bandwidth is small enough, and that the localization at low temperatures proceeds by phase-coherent backscattering off this disorder.

Four different SL's, grown under the same conditions, with the same number of SL unit cells and similar carrier densities but different miniband widths, were characterized and studied. Structural analyses showed that all four samples possessed a well-defined average SL periodicity, but with the thickness of any given layer varying randomly by ± 1 atomic monolayer about the average thickness. Evidence for a breakdown of semiclassical transport under large applied electric fields is observed. It is also observed from low-temperature magnetotransport that the layer thickness disorder gives rise to weak localization corrections to the conductivity in the smaller bandwidth SL's, but not the larger bandwidth ones. This paper expands upon previously published preliminary communications regarding high-electric-field and transverse magnetotransport experiments,[10,11] and provides a detailed discussion and analysis of the localization phenomena we have observed. To compare with the studies of Sibille *et al.*,[5] we have added one SL of comparable bandwidth to those used in Ref. 5. The organization of the paper is as follows: In Sec. II we review the relevant theoretical framework, while Sec. III deals with the sample specifications and characterization, Sec. IV presents the field-induced localization results, and Sec. V discusses

 ©1993 The American Physical Society

the magnetotransport and disorder localization. We summarize and present our conclusions in Sec. VI. In a forthcoming paper we will address the longitudinal magnetotransport results in these SL's.[12]

II. THEORY OF ELECTRON LOCALIZATION IN SUPERLATTICES

We operatively define electron localization as any situation where the probability amplitude of finding a conduction electron is peaked about a particular site or sites in a solid, as opposed to the spatially extended states of conventional Bloch behavior. The typical macroscopic manifestation of localization is a divergence in the appropriately defined resistance (or, equivalently, a vanishing conductance) under certain conditions of temperature, electric field, and magnetic field.[13] We will be concerned with two types of electron localization which, while physically distinct, meet this operative definition. The first type, electric-field-induced localization,[14] is expected to occur even in rigorously periodic lattices given appropriate field strengths and scattering times. The second, which variously goes under the names of Anderson, weak, or disorder-induced localization,[15] occurs in systems with a degree of disorder (nonperiodicity). We review here the relevant details of both types of localization as they apply to SL's. The experimental results in Sec. III and IV show that real SL's demonstrate both types of localization to varying degrees, depending on bandwidth.

A. Field-induced localization

The deceptively simple question of what happens to a Bloch electron in the conduction band of a rigorously periodic lattice in a large applied electric field, F, has a long and checkered history.[7] Large field in this sense means that the bias energy per unit cell $eV/n=eFd$ is an appreciable fraction of the bandwidth Δ, where e is the electron charge, V is the total applied voltage, n is the number of unit cells, and d is the unit-cell dimension. In the absence of any scattering, standard semiclassical theory predicts that for any nonzero F, the electron wave vector will smoothly increase toward and cross the boundary of the first Brillouin zone. In a one-dimensional reduced-zone picture, the electron will reflect off the Brillouin-zone boundary and acquire a velocity opposing its original velocity and so move toward the opposite boundary. Without scattering, such back-and-forth reflections will proceed unabated and an oscillating current will be established.[16] This ac response to a dc applied field, the Bloch oscillation, has never been observed in any lattice or superlattice. Wannier[17] proposed in 1960 that, in the presence of both a sufficiently large field F and a finite scattering time, a reflection from the Brillouin-zone edge would interfere with the forward wave and localize electrons in space. This formally results in a family of eigenfunctions of the form $\psi(z-nd)$ for integer n and an energy eigenvalue spectrum of equally spaced levels linearly dependent on F, the "Stark Ladder" $\varepsilon_n=\varepsilon_0+neFd$, where ε_0 is the energy at the band minimum. Rabinovitch and Zak[18] strongly disagreed with Wannier's analysis. They pointed out that the addition of the electric-field term $-eFz$ to the Bloch Hamiltonian both destroys the translational symmetry and introduces a sensitivity to boundary conditions, since this field potential diverges in an infinite sample. Hence, they argued, Wannier's description based on Bloch-like states and a conventional band structure was invalid. In this view, the Stark ladder spectrum still gives a formally correct set of eigenvalues, except that ε_0 takes on a continuous range of possible energies, eradicating the distinctive ladder structure. However, Koss and Lambert reported in 1972 the observation of linearly field-dependent Wannier-Stark ladder states in the optical-absorption spectra of GaAs.[19] Since 1960, this issue has been debated in the literature by various authors[20] for a quarter century. In 1986, Krieger and Iafrate[21] showed that the electric-field term in the Hamiltonian can be incorporated into a time-dependent vector potential, in analogy to the usual treatment of the magnetic field, and hence the periodicity and finiteness of the Hamiltonian is preserved. They resolved the dispute by finding the existence of the discrete Stark ladder spectrum to be an excellent approximation for normal time scales and realizable electric fields. The Stark ladder spectrum will eventually become washed out (in the manner of Zak and Rabinovitch) when the probability of field-induced interband transitions begins to strongly couple different bands and so erase the band structure, but Krieger and Iafrate found the time scale for this could be years at fields of $\sim 10^6$ V/cm.

Esaki and Tsu[22] and Tsu and Döhler[23] suggested in the 1970s that semiconductor superlattices could provide an excellent resource to experimentally investigate the issues involving field-induced localization. The larger real-space periodicity d, and hence the smaller Brillouin-zone dimension, makes it easier in principle to accelerate electrons to near the Brillouin-zone edge, compared to atomic lattices. Esaki and Tsu[19] pointed out that in a $GaAs/Ga_{1-x}Al_xAs$ SL, starting with an electron at the Brillouin-zone center $k=0$, it is possible even in the presence of scattering for the wave vector k, in an achievable field F, to extend out to an appreciable ($\sim\frac{1}{2}$) fraction of the first Brillouin-zone boundary:

$$k(F)=\frac{eF_\tau}{\hbar}\approx\frac{\pi}{2d}\ , \tag{1}$$

where τ is the shortest scattering time and the SL Brillouin zone boundaries are at $\pm\pi/2d$. For a tight-binding miniband[24] with $\varepsilon(k)=\Delta/2[1-\cos(kd)]$, the curvature of the band changes sign near $k=\pi/2d$, hence the effective band mass $m^*=\hbar^{-1}(\partial^2\varepsilon/\partial k^2)^{-1}$ changes sign, converting an electron into a hole. This hole current will subtract from the original electron current set up by the applied field and will in principle cause the differential conductivity to fall sharply, eventually becoming negative. Note that this negative differential conductivity sets in when $F\sim\hbar/\tau$, within a factor of order unity, independent of the miniband energy width Δ. Since the conductivity drops sharply, this mechanism is often described as field-induced localization by the negative effective-mass mechanism.

The negative effective-mass mechanism can occur

when the bias energy per unit cell is significantly smaller than the miniband width, i.e., $eV/n < \Delta$, so that the standard semiclassical band picture remains valid.[14] In the original work of Döhler and Tsu,[23] they argued that the onset of field-induced localization by a Wannier-Stark ladder coincides with the breakdown of band conduction. That is, if the miniband width is sufficiently small such that $eV/n \approx \Delta$ for a realizable field, then the "perturbation" energy supplied by the field is larger than the natural bandwidth, destroying band conduction. At this point spatial localization occurs; the electrons become increasingly confined to the GaAs wells and a Stark ladder energy spectrum develops. Conduction through the SL can then only proceed via interwell hopping, again causing negative differential conductivity in the SL. In this case, however, the localization potential $eV/n \propto \Delta$, in contrast to the negative effective-mass case. The Stark ladder energy levels arising mainly from the splitting of the narrow heavy-hole miniband in SL's were observed by Mendez, Agullo-Rueda, and Hong,[25] and by Voisin *et al.*[26] using photoluminesence and photoconductivity spectroscopy

In the original treatments of Refs. 22 and 23, the negative effective-mass and Wannier-Stark ladder localization mechanisms were considered distinct, and it was unclear how the two might compete in real SL's. Recently, Tsu and Esaki[7] and Capasso *et al.*[8] have presented compelling heuristic arguments that both mechanisms can be interpreted as different physical limits of the same underlying physics governing the behavior of electrons in a lattice at high electric field. The physical rationale behind this is that both field-induced localization mechanisms result directly from the Bragg condition in the periodic lattice. From this point of view, the localization is seen to arise from interfering forward and Bragg reflected waves, and the observed effect depends on the competition between the natural bandwidth, Δ, and the broadening due to scattering, $\hbar/\tau$. As emphasized in Ref. 12, as long as band conduction is valid, i.e., when $\Delta > \hbar/\tau$, then one expects scattering to limit the high-field conduction and a progressive localization begins to set in when $eV/n \sim \hbar/\tau$. The exception occurs when $\Delta \lesssim \hbar/\tau$, so that band conduction breaks down and the bandwidth, not the scattering, will limit the high-bias behavior. One should note that in practice a specific value for Δ can be specified in the design of a SL, but τ is generally not controllable. Sibille *et al.*[5] anticipated that there exists one function $V_{\rm loc}(\Delta,\tau,\varepsilon(k))$ that describes the onset of field-induced localization throughout the entire range of Δ for a given τ and $\varepsilon(k)$. The traditional notions of Wannier-Stark ladder (WSL) and negative effective-mass (NEM) mechanisms then appear as limiting behavior of $V_{\rm loc}$:

$$\lim_{\Delta\to 0} V_{\rm loc}(\Delta,\tau,\varepsilon(k)) \propto \Delta \quad ({\rm WSL})\ , \qquad \lim_{\Delta \gg \hbar/\tau} V_{\rm loc}(\Delta,\tau,\varepsilon(k)) \propto \frac{\hbar}{\tau} \quad ({\rm NEM})\ , \tag{2}$$

with some sort of crossover or coexistence regime in between. As discussed by Tsu and Esaki,[7] given a realistic τ of the order 0.1 ps quoted in Refs. 5 and 6, the crossover regime is expected to be around $\Delta \sim 10$ meV, within a factor of order unity.

B. Disorder-induced localization

The theory behind disorder-induced localization is firmly established, and a complete review giving all the relevant results for systems with isotropic Fermi surfaces in one, two, and three dimensions is given by Lee and Ramakrishnan.[27] The synthesis of SL's permits the experimenter to build in a specified type and amount of disorder in a unique manner by, for instance, varying the layer thicknesses or barrier heights, following a predetermined statistical distribution. This tunability comes at the expense of a possibly more complicated theoretical analysis, since the SL Fermi surface is either ellipsoidal or cylindrical (open), depending on the degree of anisotropy and the carrier density. Several of these possible complications have been considered theoretically by Sokoloff,[28] Das Sarma, Kobayashi, and Prange,[29] and Yang and Das Sarma.[30] Experimental and theoretical work on localization in planar transport and complications arising from the SL anisotropy was pursued by Szott, Jedrzejek, and Kirk.[31]

In the standard picture of weak localization, backscattering of electrons off the disorder decreases the absolute conductance, compared to the rigorously periodic ideal, at all temperatures. At low temperatures, it follows from Anderson's original analysis[32] that if the elastic scattering centers are located randomly in space, then the phases of the backscattered electron waves will be coherent and interfere constructively, enhancing the probability amplitude that the electron will return to where it came from, resulting in localization. (This is precisely the opposite case of a rigorously periodic system, where the reflected waves interfere destructively at low temperature, essentially canceling the backscattering and resulting in metallic behavior.) Since this phase-coherent backscattering will become more significant as incoherent inelastic-scattering processes are frozen out, the resistance diverges at very low temperatures. The definitive test of this idea is to study the resistance changes in an applied transverse magnetic field; that is, a field perpendicular to the current density, so that some component of the vector potential lies along the average current path (see Fig. 1). The integration of the vector potential into the wave-function phase will suppress the phase coherence, resulting in a decreasing resistance, i.e., a negative magnetoresistance or positive magnetoconductance, in a magnetic field at any given temperature.

The theory of disorder-induced weak localization is a scaling theory with three relevant length scales: the elastic diffusion length l_e, the inelastic diffusion length l_i, and the magnetic-field length l_H, each defined by

$$l_e = \sqrt{D\tau_e}, \quad l_i = \sqrt{D\tau}, \quad l_H = \sqrt{\hbar c/eH}\ , \tag{3}$$

where D is the electronic diffusion constant and τ is the mean scattering time. As $T \to 0$, τ_e is expected to be temperature independent, and τ_i is usually taken to increase as a power law: $\tau_i \sim T^{-p}$, where the exponent p is used to characterize the nature of the inelastic scattering. The

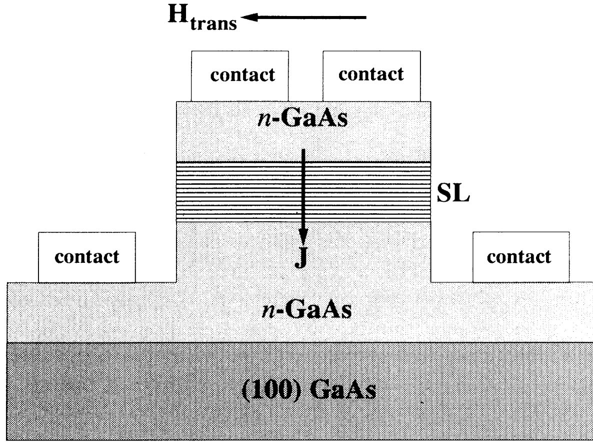

FIG. 1. Schematic illustration of a patterned superlattice mesa. For clarity, aspect ratios are not to scale. The arrows show the relative orientations of the current density J and the magnetic field H_{trans} that define the transverse orientation.

coherent backscattering necessary for weak localization is turned off at higher temperatures by inelastic scattering, so at low temperature the increase in the resistivity due to the onset of localization scales with l_i, giving, for three-dimensional (3D) systems,

$$\frac{R(T)}{R(0)} \approx 1-\alpha T^{p/2} \quad \text{as} T \to 0 \; , \tag{4}$$

where it is presumed that the coefficient α is small enough such that $\alpha T^{p/2} \ll 1$ over the relevant temperature range. The order parameter of the scaling theory is the conductance (*not* the conductivity), so that the quantitative shape of the magnetoconductance allows one to obtain l_i and l_e at any given temperature. In 3D, the expected behavior is

$$\begin{aligned} &\text{Low field:} \quad l_H \ge \sqrt{l_i l_e} \Longrightarrow \Delta G/G_0 \sim H^2 \; , \\ &\text{Midfield:} \quad \sqrt{l_i l_e} \ge l_H \ge l_e \Longrightarrow \Delta G/G_0 \sim H^{1/2} \; , \\ &\text{High field:} \quad l_e \ge l_H \Longrightarrow \Delta G/G_0 \sim \text{const} \; , \end{aligned} \tag{5}$$

where $\Delta G/G_0 = [G(H)-G(0)]/G(0)$ is the measured magnetoconductance at fixed temperature. When the diffusion constant D is primarily due to elastic scattering and so is temperature independent, one can obtain the inelastic temperature dependence by inferring l_i from the magnetoconductance at several different temperatures. Note that both the sign and the shape of the magnetoconductance are distinctive: the conductance must increase with increasing field, must have negative curvature in the midfield regime, and must saturate at high fields.

III. SAMPLE PREPARATION AND CHARACTERIZATION

The SL's used in this experiment were grown on laser-quality, semi-insulating GaAs(100) substrates at a temperature of 690 °C using standard MBE techniques.[33] A 1-μm Si-doped ($n = 10^{18}$ cm^{-3}) GaAs buffer layer was deposited first, followed by the SL, which began and ended with an undoped GaAs layer to improve contact symmetry, and capped with 0.5 μm of n^+ GaAs (see Fig. 1). Shubnikov–de Haas oscillations showed that the carrier density in the buffer layers was within 10% of the design. The SL's were composed of undoped GaAs wells and uniformly Si-doped $Ga_{0.7}Al_{0.3}As$ barriers. In each case the density of donors was adjusted so that the wells contained a mobile electron density of $\sim 10^{17}$ cm^{-3} and a Fermi energy $\varepsilon_F \approx 1.7$ meV. The samples are identified by their nominal well/barrier thicknesses, which were (in Å) 50/50, 20/80, 80/20, and 20/40, with the SL unit cell repeated 50 times. The lowest SL miniband widths calculated via a $\mathbf{k}\cdot\mathbf{p}$ approach[10] for these samples, based on the Γ-Γ offset between GaAs wells and $Ga_{0.7}Al_{0.3}As$ barriers, are 12, 18, 28, and 85 meV, respectively, so that in all cases ε_F sits near the bottom of the miniband.

Figures 2 and 3 show (a) a low-angle x-ray-diffraction pattern and (b) the SL satellites about the GaAs(200) Bragg peak from the 50/50 and 20/80 SL's using the Cu($K\alpha_1$) line from a rotating anode four-circle diffractometer. Clearly identified for both samples are the SL Bragg peaks, whose widths indicate that the average periodicity is well defined. Note that the symmetry of the 50/50 SL is such that the structure factor causes the even order indexed peaks to vanish, though this is not true for the 20/80, 80/20, or 20/40 samples.[34] By plotting the scattering wave vector $q = (4\pi/\lambda)\sin\theta$ vs the order ($h00$) of the low-angle SL Bragg peaks, one obtains from the slope of the least-squares fit line an accurate measure of the average SL period, which for the 50/50 and 20/80 samples were 102.2 and 102.8 Å, respectively,

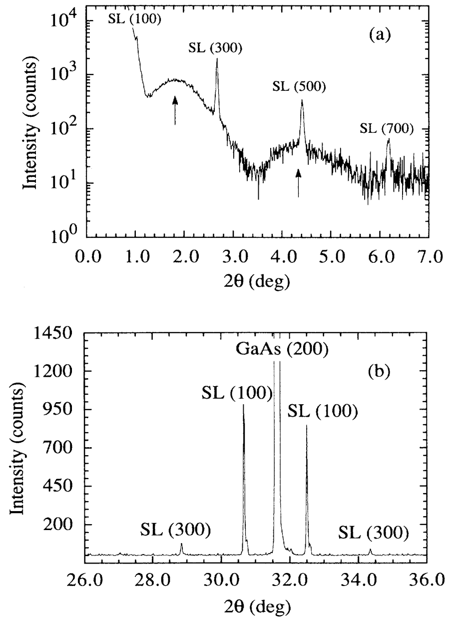

FIG. 2. (a) Low-angle 2θ x-ray-diffraction scan for the 50/50 superlattice. SL Bragg peaks are indexed. Arrows point to the peaks in the diffuse background scattering. (b) Superlattice satellite peaks around the bulk GaAs (200) Bragg peak for the same SL.

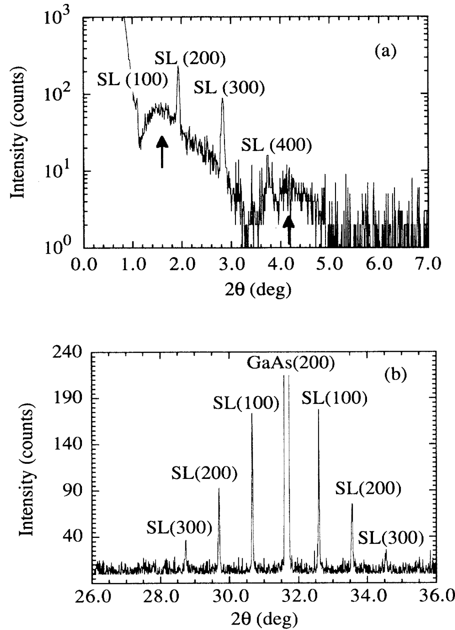

FIG. 3. (a) Low-angle 2θ x-ray-diffraction scan for the 20/80 superlattice. SL Bragg peaks are indexed. Arrows point to the peaks in the diffuse background scattering. (b) Superlattice satellite peaks around the bulk GaAs (200) Bragg peak for the same SL.

within one-half atomic unit cell of the design. The remaining SL's showed similar diffraction spectra.

In addition to the SL Bragg peaks, one can also see in Figs. 2(a) and 3(a) evidence of low-angle diffuse scattering in the form of two broad peaks near $2\theta = 1.8°$ and $4.4°$ for the 50/50 sample and near $1.6°$ and $4.2°$ for the 20/80 specimen. The origin of this diffuse scattering can be

TABLE I. Summary of the characteristics of the four superlattices studied.

SL	d (Å)	Δ (meV)	V_{loc} (volts)	l_e (Å)	l_i (Å@1.8 K)
50/50	100	12	1.3	120	2000
20/80	100	18	1.9	220	2500
80/20	100	28	3.0		
20/40	60	85	3.4		

traced back to the fact that, in standard MBE growth, there is typically a ± 1 atomic monolayer random fluctuation in the absolute thickness of any given layer. Without affecting the underlying atomic lattice spacings, this fluctuation introduces a small static disorder in the long-wavelength spatial variation of the electron density on top of the average SL periodicity. It is this frozen-in one-dimensional randomness that gives rise to the low-angle diffuse scattering, similar to a frozen quasi-1D liquid.[35] These monolayer thickness fluctuations can be directly observed in cross-section transmission electron micrographs (TEM) of these SL's, an example of which is shown in Fig. 4.

Mesas of areas 9.60×10^{-5} and 1.92×10^{-4} cm^2 were defined by wet etching down to the n^+ buffer layer. Two Au-Sn contacts were made on the top n^+ layer of each mesa and two more on the base n^+ layer to form a four-probe geometry for vertical transport (Fig. 1). For reference, the relevant characteristics for each SL are summarized in Table I. All contact resistances were confirmed to be ohmic over the relevant voltage range of ± 5 V. Current density-voltage (J-V) measurements were made with a feedback-stabilized, four-probe dc voltage supply. By direct comparison with two-probe measurements, we confirmed that the metal-semiconductor contact resistances were insignificant at all magnetic fields using the

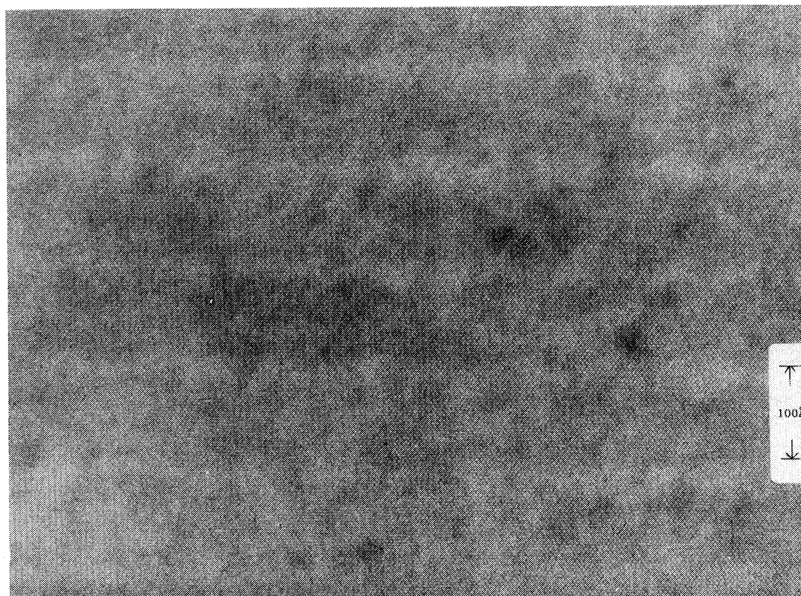

FIG. 4. High-resolution cross-sectional transmission-electron micrograph for the 20/80 superlattice.

four-probe technique. Both long (500 ms) and short (5 ms) bias durations were used to confirm the lack of heating effects. The differential conductance (dJ/dV) was measured using lock-in detection of a small ac modulation on the dc bias. Bias polarity was always referenced to the base voltage contact. Measurements were performed in a vapor-cooled insert in a liquid ^{4}He cryostat equipped with a 9-T superconducting solenoid and in a dilution refrigerator with a 12-T magnet.

IV. LOCALIZATION IN LARGE ELECTRIC FIELDS

Shown in Fig. 5 are (a) the normalized J-V data and (b) the normalized conductance dJ/dV vs V traces obtained for all four SL's at a temperature of 4.2 K. The current densities are normalized to their values at the characteristic voltage V_{loc} (defined below) so that the data from each of the four SL's could be plotted on the same graph without loss of detail; the normalization factors are given in the figure caption. Slight asymmetries with respect to bias polarity are attributable to differences in carrier density between the top and bottom contact layers. In each case the low-bias $J(V)$ is simply ohmic, implying conventional band conduction. As the voltage is increased, however, there comes a point where J fails to increase linear proportion to V. The nature of this nonlinearity is better characterized in the conductance data, where one sees that the dynamic conductance dJ/dV falls precipitously at higher bias. The strength of the nonlinearity is clearly most pronounced for the smallest bandwidth 50/50 SL, where the conductance actually crosses zero and becomes slightly negative over a small region of voltage. The nonlinearity becomes progressively less prominent as the bandwidth increases. Because the conductance drops at large electric fields, this phenomenon is described as an electric-field-induced localization of the conduction electrons. We identify a characteristic localization voltage V_{loc} with the first minimum in dJ/dV, as indicated by the arrows in Fig. 5(b). This definition makes it simple to distinguish V_{loc} unambiguously from the data, but is likely more representative of the voltage at which field-induced localization is strongest and not necessarily where it first begins to set in. From Fig. 5(b), the values of V_{loc} for 50/50, 20/80, 80/20, and 20/40 are 1.3, 1.9, 3.0, and 3.4 V, respectively (summarized in Table I), with approximately a ± 0.1-V variation among different mesas of the same nominal SL. The fact that these characteristic features occur at biases of volts rather than millivolts strongly indicates that the potential drop occurs across the SL as a whole rather than one or two unit cells, militating against high-field domain formation and double- or triple-well resonant tunneling effects.

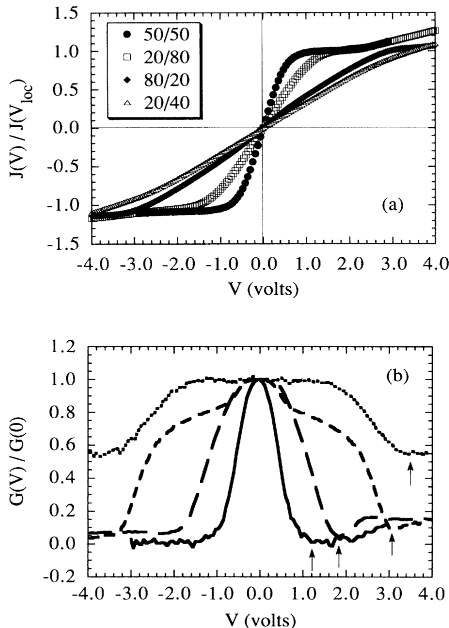

FIG. 5. (a) Normalized current density vs voltage bias characteristics for the four superlattices. Absolute current densities at V_{loc} are 80 Å/cm^2 for 50/50, 300 Å/cm^2 for 20/80, 460 Å/cm^2 for 80/20, and 495 Å/cm^2 for 20/40. (b) Normalized differential conductivity vs voltage bias for the four SL's: 50/50 (solid line), 20/80 (long dashes), 80/20 (short dashes), and 20/40 (dots). Arrows mark the definition of V_{loc} in each case.

Figure 6 shows the measured $eV_{\text{loc}}/50$, where 50 is the number of SL unit cells, against the calculated SL miniband widths. In the 10–30-meV bandwidth range, there is clear evidence for a linear dependence of V_{loc} on Δ. The line shown is a linear least-squares fit to the first three points and has a slope of approximately 2. The fact that this extrapolates to nearly $V_{\text{loc}}=0$ when $\Delta=0$ is important, since on the basis of tight-binding theory[24] a zero-width (dispersionless) band is formed of completely localized states and hence is always fully localized. (Equivalently one can regard the effective band mass in such a case as formally infinite.) However, the data point for the widest bandwidth 20/40 SL indicates that this linearity does not persist at larger bandwidths, where V_{loc} becomes nearly independent of Δ. Since V_{loc} for 20/40 is only slightly larger than for 80/20, we can infer that the turnover in $V_{\text{loc}}(\Delta)$ occurs around $\Delta=30$ meV for the SL's studied here.

We conclude that in the region of smaller bandwidths,

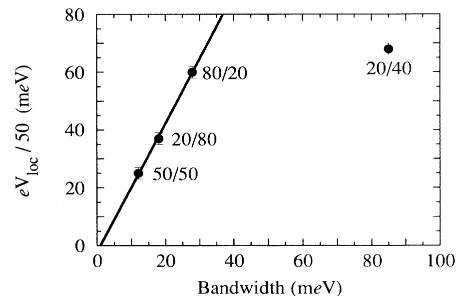

FIG. 6. Measured V_{loc} vs calculated backwidth. Error bars mark the spread of V_{loc} values measured across all mesas of each type of SL. The solid line is a least-squares fit to the first three points.

field-induced localization occurs when the bias energy per unit is of the order of the miniband width, but as the bandwidth increases field-induced localization occurs roughly independently of Δ. The linear behavior of $V_{loc}(\Delta)$ is consistent with the Tsu-Döhler model of Ref. 20, which predicts a linear dependence $eV_{loc}=gn\Delta$ where g is a factor of order unity. At larger bandwidths, the departure from linearity means that the Tsu-Döhler mechanism fails to apply. The insensitivity of V_{loc} to Δ for $\Delta>30$ meV strongly suggests that the negative effective-mass model, where to first order $eV_{loc}=gn\hbar/\tau$ independent of bandwidth, begins to dominate in this regime. In the middle bandwidths near 30 meV, where $V_{loc}(\Delta)$ turns over, the field-induced localization behavior cannot be ascribed to either mechanism individually.

The data shown here for SL's with $\Delta\geq 30$ meV are consistent with findings of Sibille *et al.*,[5] who concluded that the negative effective-mass mechanism was primarily responsible for the field-induced localization seen in their SL's with $\Delta\geq 50$ meV. In a recent work, Sibille and Palmier[36] reported that a SL with $\Delta=27$ meV showed similar bandwidth-independent field-induced localization behavior in transport, but also showed spectroscopic evidence of Stark ladder states in photoconductivity. Their finding conforms with the idea presented here that a crossover or coexistence region prevails near $\Delta\sim 30$ meV where neither the Wannier-Stark ladder nor the negative effective mass is independently defined.

Although Γ-*X* intervalley transfer will compete to some extent with field-induced localization because of the rather large fields (~20 kV/cm) involved, it is unlikely to qualitatively affect our conclusions, as discussed by Sibille *et al.*[37] With a direct-gap $Ga_{0.7}Al_{0.3}As$ barrier, rather than an indirect AlAs barrier, intervalley transfer will be naturally suppressed. Furthermore, what Γ-*X* transfer does occur will inhibit full localization in the lowest band, since electrons in localized states in the lowest band have some probability of scattering up into the second miniband, which is nearly empty and considerably wider and hence less susceptible to field-induced localization effects. Thus Γ-*X* transfer may be partially responsible for the lack of a distinct negative dJ/dV region near V_{loc} in Fig. 5, in contrast to the data of Ref. 6, where a *p-i-n* junction construction enabled use of fields ~10 times smaller, effectively eliminating complications resulting from intervalley transfer. However, V_{loc} is still an appropriate characteristic voltage for the field-induced localization process.

The data of Fig. 6 support the recent ideas of a unified picture of field-induced localization, where the Wannier-Stark ladder and negative effective-mass mechanisms are no longer thought of as distinct processes, but are more appropriately regarded as the same underlying physical phenomenon manifested in two different physical limits. Although Tsu and Esaki[7] convincingly argued on physical grounds that some type of crossover behavior must occur when $\Delta\sim\hbar/\tau$, up to now no microscopic theoretical analysis has either calculated nor even fully justified the form of the unified function $V_{loc}(\Delta,\tau,\varepsilon(k))$. However, the data presented here combined with the recent experimental work of Refs. 5 and 6 lend this idea both credence and empirical support.

V. DISORDER-INDUCED LOCALIZATION

The temperature dependence of the low-bias (ohmic regime) resistance R is shown in Fig. 7 for the four SL's. There are three regions involved. At high temperature (20 K $<T<$ 100 K), R increases by about 5% as T is lowered, so that $dR/dT<0$. Such behavior is usually indicative of inelastic-scattering processes promoting electrons across the barriers, either by thermionic emission or by assisted hopping.[38] For 5 K $<T<$ 20 K, R flattens out and becomes nearly independent of T. Here the inelastic scattering is being frozen out, and a transition to quantum tunneling, which is temperature independent,[39] occurs. Below ~5 K in the smallest bandwidth 50/50 sample there is a weak but distinct upturn in the resistance, which we shall argue is due to weak localization corrections caused by disorder-induced coherent backscattering.

Figure 8 shows the low-temperature resistance upturn for the 50/50 SL in greater detail from 7 to 20 mK in both zero applied magnetic field and an applied transverse field of 5 T. As can be seen from the figure, the resistance increase is almost completely suppressed by application of the magnetic field. At any given temperature, the resistance decreases with an applied transverse field, so that the transverse magnetoresistance $\Delta R/R_0=[R(H)-R(0)]/R(0)$ is negative. We note that no magnetic impurities were evident in any of the SL's studied; susceptibility measurements up to 5 T revealed only standard semiconductor Landau diamagnetism, as shown by the inset of Fig. 8. As discussed in Sec. III, the negative magnetoresistance constitutes a clear signal that the low-temperature resistance upturn is being caused by phase-coherent backscattering off of disorder in the SL. Figure 9 show the magnetoresistance as a function of H at fixed temperature (2 K) for all four SL's. The two smaller bandwidth samples 50/50 and 20/80 show clear negative magnetoresistance, though with different magnitudes and characteristic fields. The magnetoresistance for 50/50 saturates at about -0.3% above ~4.5 T, and the magnetoresistance for 20/80 saturates around -0.15% above ~1.5 T at this temperature. The two wider bandwidth SL's 80/20 and 20/40 do not show

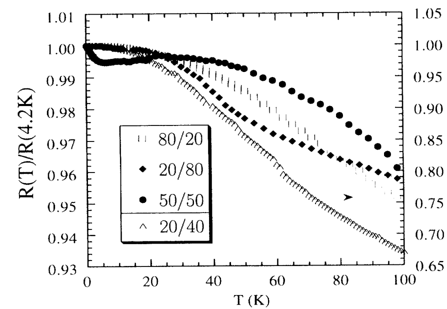

FIG. 7. Temperature dependence of the resistances of all four samples below 100 K.

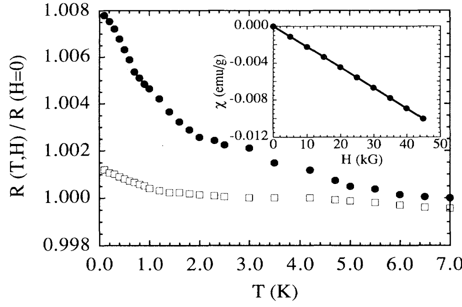

FIG. 8. Low-temperature behavior of the resistance of the 50/50 sample in zero applied field (black circles) and in a transverse field of 5 T (open squares). Inset: Susceptibility vs field for the 50/50 SL. The solid line is a least-squares fit.

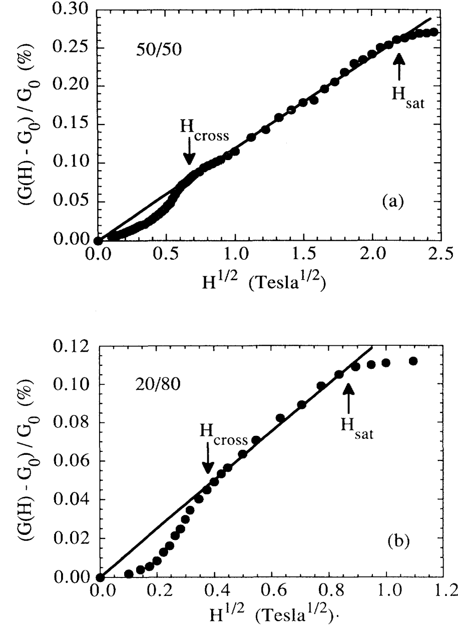

FIG. 10. Transverse magnetoconductance vs square root of the field at $T=1.8$ K for (a) the 50/50 sample and (b) the 20/80 sample. The lines are least-squares fits to the middle range of data points. The arrows mark the characteristic fields H_{cross} and H_{sat}.

negative magnetoresistance. The resistance of the 80/20 sample is virtually field independent, while the widest bandwidth 20/40 SL shows a positive magnetoresistance of a few percent. Note that the trend is for the magnetoresistance to become increasingly positive as bandwidth increases. Despite the fact that x-ray studies show that all these SL's share approximately the same type and degree of disorder, only the smaller bandwidth samples appear to evidence significant weak-localization effects. This may be expected since the effective band mass becomes heavier as the bandwidth becomes smaller, leading to greater susceptibility to any localization effects. Szott, Jedrzejek, and Kirk[31] have previously established that the conductivity tensor in SL's is bandwidth dependent. These data provide a direct study of the influence of bandwidth on the disorder-induced quantum corrections to the transport behavior.

With $\varepsilon_F \approx 1.7$ meV, the Fermi surfaces in all four SL's are closed ellipsoids rather than open cylinders. In this case, these SL's are more properly regarded as three dimensional, so we shall use the results of the scaling theory of weak localization appropriate to 3D.[26] While this theory is strictly applicable only to a spherical Fermi surface, we assume that the anisotropy introduces no qualitative corrections, although this topic is currently under theoretical investigation by several groups.[25–27]

Following Eq. (3), we plot in Fig. 10 the transverse *magnetoconductance* $\Delta G(H)/G_0$ of the 50/50 and 20/80 specimens vs $H^{1/2}$. For both samples, at high fields $\Delta G(H)/G_0$ saturates. There is a midfield regime where $\Delta G(H)/G_0$ fits reasonably well to an $H^{1/2}$ line, and in the low-field regime the data fall below the $H^{1/2}$ line. We note that the behavior as $H \to 0$ does not behave as $\sim H^2$, the data coming in more cusplike. This behavior, which is supposed to be independent of dimensionality, is apparently common in two- and three-dimensional weak-localization systems[40,41] and is not presently understood. Nevertheless, one can identify two characteristic fields: a crossover field H_{cross}, where the low-field data intersects the $H^{1/2}$ line, and a saturation field H_{sat}. From the data of Fig. 10, we find

$$H_{\text{cross}} \approx 0.28 \text{ T}, \quad H_{\text{sat}} \approx 4.4 \text{ T} \quad \text{for the 50/50 SL},$$

$$H_{\text{cross}} \approx 0.12 \text{ T}, \quad H_{\text{sat}} \approx 1.3 \text{ T} \quad \text{for the 20/80 SL},$$

where there is a slight ($\sim 10\%$) dependence on what range of data points we choose to use in the $H^{1/2}$ line fit. Using Eq. (3), we can then derive the relevant length scales:

$$l_e \approx 120 \text{ Å}, \quad l_i \approx 2000 \text{ Å} \quad \text{for the 50/50 SL},$$

$$l_e \approx 220 \text{ Å}, \quad l_i \approx 2500 \text{ Å} \quad \text{for the 20/80 SL},$$

at 1.8 K. These values are summarized in Table I. The elastic mean free path in both cases is comparable to one or two SL unit cells, which is consistent with the notion that fluctuations in the layer-to-layer thicknesses are the dominant form of disorder in this experiment.

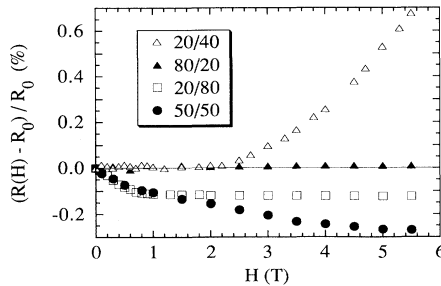

FIG. 9. Transverse magnetoresistance vs applied field for all four samples at $T=2$ K.

The inelastic-scattering behavior can be deduced independently from the low-temperature dependence of both the resistance R and the inelastic length $l_i=(D\tau_i)^{1/2}$, as shown in Fig. 11. A power-law fit to $R(T)$ and $l_i(T)$ in the range of 0.1–2 K shows that a linear power is most appropriate, so by Eqs. (3) and (4) the inelastic scattering time $\tau_i \sim T^p$ with $p=2$ as $T\rightarrow 0$. This value of p is indicative of electron-electron scattering in 3D, where a simple phase-space argument gives $\tau_i \sim T^2$, so that the dominant mechanism of inelastic phase relaxation at low temperature is most likely electron-electron scattering. It is interesting to compare this result to the work of Lin *et al.*[41] on weak localization in a 2D electron gas in a GaAs/$Ga_{0.7}Al_{0.3}As$ heterostructure. They found that at low temperature $p=1$, which is consistent with electron-electron scattering in 2D, where the phase-space integral yields $\tau_i \sim (T \ln T)^{-1} \sim T^1$ over the temperature range achievable in practice. It is unsurprising that the low-temperature phase relaxation mechanism is the same in both systems, since the materials are the same, and the carrier densities are very similar.

One can obtain an estimate for the perturbation energy associated with the layer thickness disorder by considering the difference in lowest-energy states between two square GaAs wells separated by a $Ga_{0.7}Al_{0.3}As$ barrier, where one well is one atomic monolayer thicker than the other. For the 50/50 case, this yields an energy difference of $\Delta\varepsilon \sim 1.5$ meV. Since this perturbation is an order of magnitude less than the miniband width for the 50/50 SL, the band structure should still form with only quantitative corrections from the ideal case. The main conceptual modification introduced by the disorder is not in the formation of the band itself but in the introduction of a conduction-band mobility edge μ_e. Physically it is expected that, within a factor of order unity, $\mu_e \sim \Delta\varepsilon$, since both describe the degree of disorder in terms of an energy perturbation.[42] Of direct relevance is the fact that μ_e is comparable to ε_F, meaning that the smallest bandwidth SL is on the borderline of a disorder-induced metal-insulator transition. These estimates of the disorder-induced perturbations energies are consistent with the measured low-temperature magnetoresistive behavior.

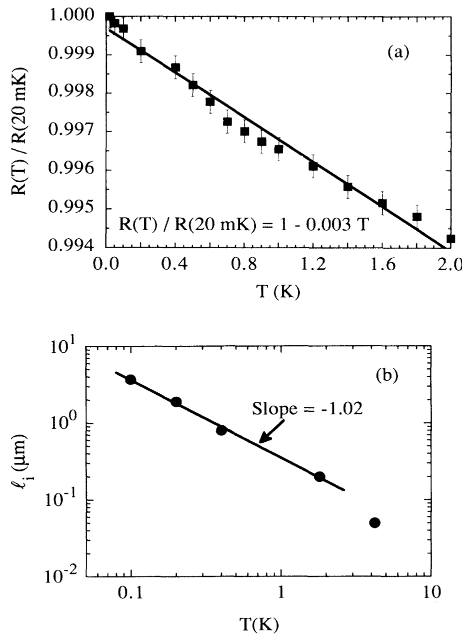

FIG. 11. (a) Low-temperature resistance vs temperature for the 50/50 sample. The line is a least-squares power-law fit. (b) Low-temperature dependence of the inelastic diffusion length. The solid line is the fit to the lowest four temperature data points.

VI. CONCLUSION

We have studied the competition between electronic conduction and localization in a set of GaAs/$Ga_{0.7}Al_{0.3}As$ superlattices, where the effects of miniband width and disorder can be quantified in a manner not otherwise possible. Experimental observation of two physically distinct types of localization has been made. Electric-field-induced localization is evident by a sharp drop-off in the dynamic conductivity dJ/dV at applied biases of 1–4 V, with a characteristic localization voltage V_{loc} defined as the first minimum in dJ/dV. At smaller minibandwidths Δ of between 10 and 30 meV, V_{loc} is measured to be linearly proportional to the bandwidth, which is consistent with a breakdown in bandlike transport caused by the formation of Wannier-Stark ladder states. The linear behavior of $V_{loc}(\Delta)$ does not persist to larger Δ, however. For $\Delta \geq 30$ meV, V_{loc} becomes only very weakly dependent on bandwidth, which is more appropriate to a negative effective-mass model. The results support the heuristic notion that there exists only one function $V_{loc}(\Delta,\tau,\varepsilon(k))$ that completely describes the behavior of electrons in a SL at high electric fields, and that the Wannier-Stark ladder and negative effective-mass mechanisms are manifestations of this function in the different physical regimes of $\Delta \ll \hbar/\tau$ and $\Delta \gg \hbar/\tau$, respectively, with a crossover regime in between. The data imply that in our SL's this crossover occurs around $\Delta \sim 30$ meV.

Structural studies of the SL's give evidence of a remnant disorder resulting from atomic monolayer differences in the absolute thickness from one SL unit cell to the next, and the localization effects due to this disorder are apparent at low temperatures. In the smaller bandwidth samples, a weak increase in the resistance as $T\rightarrow 0$ can be suppressed by application of a transverse magnetic field. This characteristically temperature- and field-dependent negative magnetoresistance shows that the resistance increase is due to quantum phase-coherent backscattering off the static spatial disorder in the SL potential. These weak-localization corrections to the transport are absent in the larger bandwidth samples, despite similar types and degrees of disorder, showing unambiguously that narrower bandwidths are more susceptible to disorder-induced localization effects. Length scales and their temperature dependencies derived from quantitative fitting of the magnetoresistance data to the scaling theory

of weak localization show that the mean elastic-scattering length is of the order of one or two SL unit cells, consistent with the layer thickness variations, and that the main mechanism of inelastic phase relaxation at low temperature is through electron-electron scattering. The SL system is a unique arena in which the type and distribution of the disorder can be identified, and the effect of bandwidth can be controlled and studied.

ACKNOWLEDGMENTS

We thank K. Woodruff and J. Ramdani for help with lithography, J. Bennett and M. J. Higgins for technical assistance, T. Thio for use of the dilution refrigerator, and P. A. Wolff and N. Wingreen for useful discussions. The SL's were grown by APA Optics, Inc., and TEM studies were done at N. C. State University.

[1]L. Esaki and L. L. Chang, Phys. Rev. Lett. **33**, 495 (1974).
[2]L. Esaki, in *Synthetic Modulated Structures,* edited by L. Chang and B. C. Giessen (Academic, New York, 1985).
[3]Federico Capasso, MRS Bull. **26**, 23 (1991).
[4]J. L. Jewell *et al.*, IEEE J. Quantum Electron. **27**, 1332 (1991).
[5]A. Sibille, J. F. Palmier, H. Wang, and F. Mollot, Phys. Rev. Lett. **64**, 52 (1990).
[6]Fabio Beltram *et al.*, Phys. Rev. Lett. **64**, 3167 (1990).
[7]R. Tsu and L. Esaki, Phys. Rev. B **43**, 5204 (1991).
[8]F. Capasso *et al.*, Phys. Rev. Lett. **55**, 1152 (1985).
[9]A. Chomette, B. Deveaud, A. Regreny, and G. Bastard, Phys. Rev. Lett. **57**, 1464 (1986).
[10]Mark Lee and S. A. Solin, Solid State Commun. **83**, 673 (1992).
[11]Mark Lee, S. A. Solin, and D. Hines, *Proceedings of the 21st International Conference on the Physics of Semiconductors,* edited by P. Jiang and H. Zheng (World Scientific, Singapore, 1992), p. 967.
[12]Mark Lee, S. A. Solin, and P. A. Wolff (unpublished).
[13]G. Bergmann, Phys. Rep. **107**, 2 (1984).
[14]Federico Capasso *et al.*, in *Resonant Tunneling in Semiconductors,* edited by L. L. Chang (Plenum, New York, 1991).
[15]T. V. Ramakrishnan, in *The Metallic and Nonmetallic States of Matter,* edited by P. P. Edwards and C. N. R. Rao (Taylor and Francis, London, 1985).
[16]See, for example, N. W. Ashcroft and N. D. Mermin, *Solid State Physics* (Saunders College, Philadelphia, 1976), p. 224.
[17]Gregory H. Wannier, Phys. Rev. **117**, 432 (1960).
[18]A. Rabinovitch and J. Zak, Phys. Rev. B **4**, (1971).
[19]Robert W. Koss and L. M. Lambert, Phys. Rev. B **5**, 1479 (1972).
[20]See, for example, D. E. Aspnes, Phys. Rev. **166**, 921 (1968); W. Shockley, Phys. Rev. Lett. **28**, 349 (1972), and works cited in Refs. 7, 18, and 21.
[21]J. B. Krieger and G. J. Iafrate, Phys. Rev. B **33**, 5494 (1986).
[22]L. Esaki and R. Tsu, IBM J. Res. Dev. **14**, 61 (1970).
[23]R. Tsu and G. Döhler, Phys. Rev. B **12**, 680 (1975).
[24]W. A. Harrison, *Solid State Physics* (Dover, New York, 1979), p. 151.
[25]E. E. Mendez, F. Agullo-Rueda, and J. M. Hong, Phys. Rev. Lett. **60**, 2426 (1988).
[26]P. Voisin *et al.*, Phys. Rev. Lett. **61**, 1639 (1988).
[27]P. A. Lee and T. V. Ramakrishnan, Rev. Mod. Phys. **57**, 287 (1985).
[28]J. B. Sokoloff, Phys. Rev. B **22**, 5823 (1980).
[29]S. Das Sarma, Akiko Kobayashi, and R. E. Prange, Phys. Rev. Lett. **56**, 1280 (1986).
[30]S.-R. Eric Yang and S. Das Sarma, Phys. Rev. B **37**, 10090 (1988).
[31]W. Szott, C. Jedrzejek, and W. P. Kirk, Phys. Rev. B **40**, 1790 (1989); Phys. Rev. Lett. **63**, 1980 (1989).
[32]P. W. Anderson, Phys. Rev. **109**, 1492 (1958).
[33]See, for example, *The Technology and Physics of Molecular Beam Epitaxy,* edited by E. H. C. Parker (Plenum, New York, 1985).
[34]A. Guinier, *X-Ray Diffraction* (Freeman, San Francisco, 1963), p. 83.
[35]Reference 34, p. 55.
[36]A. Sibille and J. F. Palmier, Appl. Phys. Lett. **457**, 60 (1992).
[37]A. Sibille *et al.*, Phys. Rev. B **39**, 6272 (1989).
[38]S. M. Sze, *Physics of Semiconductor Devices* (Wiley, New York, 1981), p. 254.
[39]E. L. Wolf, *Principles of Electron Tunneling Spectroscopy* (Oxford University Press, Oxford, 1985).
[40]D. J. Bishop, R. C. Dynes, and D. C. Tsui, Phys. Rev. B **26**, 773 (1982); G. Bergmann, Phys, Rep. **107**, 2 (1984).
[41]B. J. F. Lin *et al.*, Phys. Rev. B **29**, 927 (1984).
[42]P. A. Wolff (private communication).

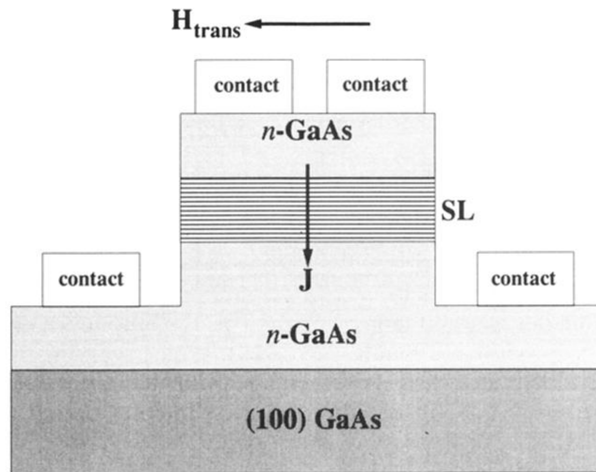

FIG. 1. Schematic illustration of a patterned superlattice mesa. For clarity, aspect ratios are not to scale. The arrows show the relative orientations of the current density J and the magnetic field $H_{\rm trans}$ that define the transverse orientation.

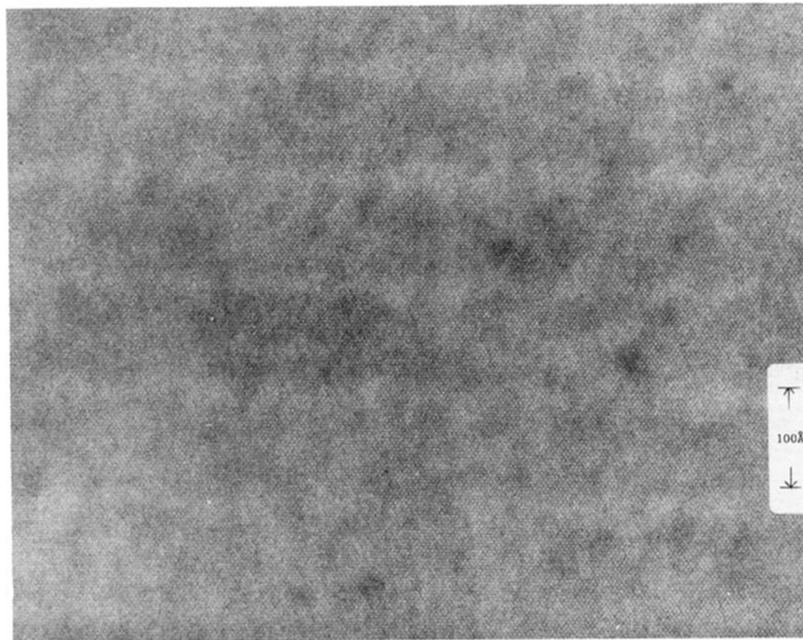

FIG. 4. High-resolution cross-sectional transmission-electron micrograph for the 20/80 superlattice.